A QSFDI based Laplacian Discretisation for Modelling Wave-Structure Interaction using ISPH

Ningbo Zhang[a], Shiqiang Yan[a,*], Qingwei Ma[a,b] , Xing Zheng[b]

a School of Mathematics, Computer Science and Engineering, City, University of London, London, UK

b College of Shipbuilding Engineering, Harbin Engineering University, Harbin, Heilongjiang, China

* Author of Correspondence. Email: shiqiang.yan.1@city.ac.uk

Abstract

The incompressible Smoothed Particle Hydrodynamics (ISPH) is one of the most popular Lagrangian particle methods for modelling wave-structure interactions. It solves the unsteady Navier-Stokes and continuity equations using the projection method, in which solving the pressure Poisson's equation (PPE) plays a critical role. To discretise the PPE, the quadric semi-analytical finite difference interpolation scheme (QSFDI) has been developed recently and the relevant patch test has demonstrated its superiority over existing schemes at a similar accuracy level in terms of the convergence and robustness. In this paper, the QSFDI is adopted by the ISPH for discretising the Laplacian operator in the PPE. The developed scheme (ISPH_QSFDI) is then applied to various cases with wave propagations and their interaction with structures. For the purpose of comparison, other Laplacian discretisation schemes, including the classic scheme widely adopted by the ISPH, the CSPM and the CSPH2Γ, have also been considered. Except the Laplacian discretisation, other numerical implementations of the ISPH, e.g. the gradient/divergence estimation and the treatment of the boundary conditions, are kept the same. The convergence, accuracy and robustness of these schemes are analysed with reference to either analytical solutions or experimental data. The results demonstrate that the present ISPH_QSFDI results in more accurate results with the same number of particles and costs less computational time to achieve a specific accuracy, compared other schemes, although the convergence rate of the ISPH_QSFDI seems to be one-order lower than the theoretical patch test due.

Commented [ZN1]: Reviewer 1: Q2

Commented [YS2]: Reviewer 2: Q2

Keywords: ISPH; QSFDI; Laplacian Operator; PPE; wave-structure interaction

1. Introduction

The wave-structure interaction is one of the fundamental problems for many coastal and offshore practical applications such as the design of breakwaters and sea walls. The Smoothed Particle Hydrodynamics (SPH)（Lucy, 1977; Gingold and Monaghan, 1977) is a Lagrangian meshless method and has been successfully applied in wide range of problems involving waves and their interaction with structures in recent years. The SPH

discretizes the the computational domain by particles, which carry field variables such as the pressure, density and velocity, and move in a Lagrangian way.

There are mainly two streams of SPH methods when being applied to modelling water waves and wave-structure interactions. One is the weakly compressible SPH (WCSPH), in which the fluid is considered to be weakly compressible and the pressure is evaluated by the equation of state related to the fluid density. The other one is the incompressible SPH (ISPH) proposed by Shao and Lo (2003) using the projection method (Cummins and Rudman, 1999). In the ISPH, the fluid is incompressible and the pressure is evaluated by solving a Poisson equation of pressure (PPE). The WCSPH does not need to solve the PPE and thus is relatively easier to be implemented compared with the ISPH. However, the WCSPH shows some weaknesses during its applications to the wave-structure interactions (Rafiee et al., 2012; Zhang et al., 2019), e.g. the significant spurious pressure fluctuations, although certain numerical techniques have been proposed to improve its performance (Inutsuka 2002; Antuono et al, 2010). The ISPH has also been widely applied for modelling the wave propagation and interaction with structures (Lind et al., 2012; Zheng et al., 2014; Gui et al., 2015; Liang et al., 2017; Khayyer et al., 2017b; Khayyer et al., 2018; Khayyer et al., 2021). Compared with the conventional WCSPH, the ISPH has shown several superiorities. According to Lee et al. (2008), the ISPH may lead to more accurate results than the WCSPH for a given particle resolution. Violeau and Leroy (2015) have shown that the time step used by the ISPH can be five times larger than the WCSPH. In addition, the ISPH has better volume conservation properties (Gotoh and Khayyer, 2016). Such superiorities may be limited by the range of the applications and considerable developments have been done to improve the computational performance of ISPH. Typical examples include the Higher order Source term (HS), Higher order Laplacian (HL), Error Compensating Source (ECS), Dynamic Stabilizer (DS) and pressure Gradient Correction (GC) (Khayyer et al., 2017a), the corrected Taylor series consistent pressure gradient models Eulerian-Lagrangian ISPH (Fourtakas et al., 2018), background mesh scheme (Wang et al., 2019), symmetric SPH (SSPH) method (Zhang and Batra, 2009), pseudo-spectral incompressible smoothed particle hydrodynamics (FFT-ISPH) (Rogers et al., 2021) and the implicit consistency correction scheme (Sibilla, 2015). It is also widely recognized that numerical schemes to discretize the PPE, including the Laplacian operator, are critical for securing a satisfactory accuracy, convergence and robustness of the ISPH. The main challenges of development and application of such schemes is largely caused

Commented [ZN3]: Reviewer 2: M4

Commented [ZN4]: Reviewer 1: Q7

Commented [ZN5]: Reviewer 2: Q3

Commented [ZN6]: Handling Editor: Q5

Commented [ZN7]: Reviewer 2: Q6

by the irregular particle distribution (Quinlan et al., 2006). When modelling the wave-structure interactions, the particles move following the material velocity and consequently are distributed irregularly even they are distributed evenly and regularly at the start of the simulation. This limits the applications of high-order finite difference schemes which require regular and even particle distribution. Detailed review on the such schemes can be found in Ma et al. (2016) and Yan et al. (2020) and will not be repeated here.

However, discussions on some Laplacian discretisation schemes, which have shown their satisfactory convergence and accuracy for irregular particle distributions, are included here for completeness. These include the CSPM proposed by Chen *et al.* (1999), a scheme proposed by Fatehi and Manzari (2011) and developed from the Brookshaw's scheme (Brookshaw, 1985), in which an error compensation is introduced, the LSMPS method developed by Tamai and Koshizuka (2014) by using the moving least squares (MLS) algorithm, LP-MPS proposed by Tamai *et al.* (2017) based on the weighted least squares (WLS) algorithm. Although the CSPM, LP-MPS and quadric LSMPS have a higher convergent rate compared with some schemes (Cummins and Rudman, 1999; Lo and Shao, 2002; Hu and Adams, 2007; Khayyer and Gotoh, 2012) that converge at a rate less than first order for estimating the Laplacian of a given function (Schwaiger, 2008; Zheng *et al.*, 2014), these schemes require the high computational cost on inversing matrices at all particles. To overcome this limitation, Schwaiger (2008) proposed a CSPH2Γ scheme, which is based on the CSPM but reduces the sizes of inversed matrices. However, the CSPH2Γ scheme downgrades the accuracy because of ignoring the cross-derivative terms of the 2nd derivatives. By adopting the principle of the linear semi-analytical finite difference interpolation (SFDI), we developed a quadric version, which is referred to as the QSFDI, for Laplacian discretization (Yan et al, 2020). The QSFDI can achieve the same degree of the convergent rate as the best schemes available to date, e.g., the CSPM, LP-MPS and quadric LSMPS, but requires inversion of significant lower order matrices, i.e., 3×3 for 3D cases, compared with 6×6 or 10×10 in the schemes with the best convergent rate. Systematic patch tests have been carried out for either estimating the Laplacian of given functions or solving Poisson's equations using disordered particles (Yan et al, 2020). The results suggested that the QSFDI requires considerably less computational time to achieve the same accuracy, particularly for estimating the Laplacian of given functions, compared with other schemes used in the patch tests. However, its performance on

Commented [ZN8]: Reviewer 2: Q4

Commented [YS9]: Reviewer 2: Q5

modelling practical problems needs to be further evaluated.

In this paper, the QSFDI is first implemented in the ISPH for discretising the Laplacian operator in the PPE. The performance of the present ISPH with QSFDI (ISPH_QSFDI) in terms of accuracy, convergence and robustness is assessed by using various practical problems. For the purpose of comparison, other schemes developed for SPH applications, including the classic ISPH scheme, the CSPM and CSPH2Γ, have been considered in the present comparative study. It shall be noted that the QSFDI (Yan et al, 2020) includes consistent schemes for numerical interpolation and gradient (spatial derivative) estimations, which can be implemented in the ISPH procedures, e.g., the treatment of the boundary condition, the calculation of pressure gradient. However, these are not implemented in this paper in order to focus our evaluation on discretizing the Laplacian operator.

2. Brief of ISPH Algorithms

For completeness, a brief introduction of the ISPH algorithms, spatial derivative approximations and boundary treatments is given here. More details can be found in Zheng et al. (2014). The governing equations are the mass and momentum conservation equations given below,

$$\frac{D\mathbf{u}}{Dt} = -\frac{\mathbf{1}}{\boldsymbol{\rho}}\nabla P + \mathbf{g} + \nu\nabla^2\mathbf{u} \quad (1)$$

$$\nabla \cdot \mathbf{u} = 0 \quad (2)$$

where ∇ is the spatial differential operator; $\rho$is the fluid density; $\mathbf{u}$ is the fluid velocity; P is the pressure; $\mathbf{g}$ is the gravitational acceleration; ν is the kinematic viscosity; t is the time and D/Dt is material derivative following the motion of the fluid particle. Eqs. (1) and (2) are discretised by Lagrangian particles and solved by the projection method, briefed below.

Assuming the position ($\mathbf{r}^t$) and the velocity ($\mathbf{u}^t$) of fluid particles are known at time t, the intermediate fluid velocity $\mathbf{u}^*$ is predicted by considering the acceleration terms in the right-hand side of Eq. (1) except the pressure gradient term, i.e. $\mathbf{u}^* = \mathbf{u}^t + (\mathbf{g} + \nu\nabla^2\mathbf{u}^t)\Delta t$, where Δt is the time step size and is determined dynamically by satisfying the CFL (Courant-Friedrichs-Lewy) condition (Shao and Lo, 2003). The intermediate position vector of the particle $\mathbf{r}^*$ is obtained by use of the $\mathbf{r}^t + \mathbf{u}^*\Delta t$. Then, the pressure at the new time step, $P^{t+\Delta t}$, can be estimated using the intermediate

Commented [ZN10]: Reviewer 2: Q11

Commented [ZN11]: Reviewer 2: Q14

density and velocity,

$$\nabla^2 P^{t+\Delta t} = \alpha \frac{\rho - \rho^*}{\Delta t^2} + (1-\alpha)\frac{\rho \nabla \cdot \mathbf{u}^*}{\Delta t} \quad (3)$$

in which α is the blending coefficient and taken as 0.01 in this paper; the intermediate fluid density ρ^* at any fluid particle i can be calculated by $\sum_{j=1}^{N} m_j W(\mathbf{r}_{ij})$ where j indicates one of N neighbouring particle of i, and $W(\mathbf{r}_{ij})$ is a kernel function corresponding to the position vector $\mathbf{r}_{ij} = \mathbf{r}_i - \mathbf{r}_j$. Similar to Lo and Shao (2002), the solid boundaries are also simulated by particles and mirror particles are placed outside the solid walls. For the particles on the solid boundary, the following conditions (Ma and Zhou, 2009) should be satisfied

$$\mathbf{u} \cdot \mathbf{n} = \mathbf{U} \cdot \mathbf{n} \quad (4)$$

$$\mathbf{n} \cdot \nabla P = \rho(\mathbf{n} \cdot \mathbf{g} - \mathbf{n} \cdot \dot{\mathbf{U}}) \quad (5)$$

where $\mathbf{n}$ is the unit normal vector of the solid boundary; $\mathbf{U}$ and $\dot{\mathbf{U}}$ are the velocity and acceleration of the solid boundary. The dynamic boundary condition on the free surface is,

$$P = 0 \quad (6)$$

In order to apply Eq. (6), particles on the free surface should be identified firstly. This paper adopts the method proposed by Zheng et al. (2014), which introduces auxiliary functions related to the particle distribution in the influence domain of each fluid particle and the corresponding particle density. More details can be found in Zheng et al. (2014). After Eq. (3) is solved, the velocity and density at $t + \Delta t$ is corrected by considering the fraction of the acceleration due to the gradient of $P^{t+\Delta t}$.

Within each time step, the velocity divergence and viscous term need to be estimated, respectively, by classic SPH formulations (Cleary and Monaghan, 1999; Monaghan, 2005; Shao and Lo, 2003), and the pressure gradient by the SFDI (Ma, 2008; Zheng et al., 2014),

$$\nabla \cdot \mathbf{u}_i = -\frac{1}{\rho_i}\sum_{j=1}^{N} m_j(\mathbf{u}_i - \mathbf{u}_j) \cdot \nabla_i W(\mathbf{r}_{ij}) \quad (7)$$

$$\nabla \cdot (\nu_i \nabla \mathbf{u}_i) = \sum_{j=1}^{N} 8 m_j \left(\frac{\nu_i + \nu_j}{\rho_i + \rho_j} \frac{\mathbf{u}_{ij} \cdot \mathbf{r}_{ij}}{r_{ij}^2 + \eta^2}\right) \cdot \nabla_i W(\mathbf{r}_{ij}) \quad (8)$$

$$\nabla P_i = \sum_{j=1, j\neq i}^{N} \frac{n_i^{x_k} B_{ij}^{x_m} - n_i^{x_y} B_{ij}^{x_k}}{n_i^x n_i^y - n_i^{xy} n_i^{xy}} (P_j - P_i) \quad (9)$$

where m is the particle mass; η is the small number to prevent singularity; $\mathbf{u}_{ij} = \mathbf{u}_i - \mathbf{u}_j$ and the kernel function $W(\mathbf{r}_{ij})$ is taken as the cubic B-spline kernel proposed by

Commented [ZN12]: Reviewer 1: Q3
Handling Editor: Q6

Commented [ZN13]: Reviewer 2: Q11

Commented [ZN14]: Reviewer 2: Q14

Commented [ZN15]: Reviewer 2: M7

Commented [ZN16]: Handling Editor: Q1

Monaghan and Lattanzio (1985) in this paper. In Eq. (9),

$$n_i^{xy} = \sum_{j=1,j\neq i}^{N} \frac{\left(\mathbf{r}_j^{x_m}-\mathbf{r}_i^{x_m}\right)\left(\mathbf{r}_j^{x_k}-\mathbf{r}_i^{x_k}\right)}{\left|\mathbf{r}_{ij}\right|^2} W(\mathbf{r}_{ij}),$$

$$n_i^{x_m} = \sum_{j=1,j\neq i}^{N} \frac{\left(\mathbf{r}_j^{x_m}-\mathbf{r}_i^{x_m}\right)^2}{\left|\mathbf{r}_{ij}\right|^2} W(\mathbf{r}_{ij}) \text{ and}$$

$$B_i^{x_m} = \sum_{j=1,j\neq i}^{N} \frac{\left(\mathbf{r}_j^{x_m}-\mathbf{r}_i^{x_m}\right)}{\left|\mathbf{r}_{ij}\right|^2} W(\mathbf{r}_{ij}),$$

in which $x_m = x$ when $x_k = y$ or $x_m = y$ when $x_k = x$, and $\mathbf{r}^{x_m}$ is the component of the position vector in x_m direction.

For solving the PPE (Eq. (3)), different schemes have been developed to discretise the Laplacian operator and the following classic scheme is commonly used,

$$\nabla\cdot\left(\frac{1}{\rho}\nabla P_i\right) = \sum_{j=1}^{N} \frac{8m_j}{(\rho_i+\rho_j)^2} \frac{(P_i-P_j)\mathbf{r}_{ij}}{r_{ij}^2+\eta^2}\cdot\nabla_i W(\mathbf{r}_{ij}) \quad (10)$$

However, the accuracy of the ISPH may be improved by replacing Eq. (10) with other schemes, in particular when the particles suffer from distortion and clustering in violent water wave problems (Zheng *et al.*, 2014). For this purpose, some schemes for the Laplace discretisation have been proposed, as indicated in the Introduction. One is the CSPM scheme developed by Chen *et al.* (1999) and reads

$$\nabla^2 P_i = 2\boldsymbol{I}_{\text{CSPM}}^{\text{T}}\boldsymbol{M}_{2,\text{CSPM}}^{-1}\left(\sum_{j=1}^{N}\frac{m_j}{\rho_j}(P_j-P_I)\nabla^{(2)}W(\mathbf{r}_{ji}) - \sum_{j=1}^{N}\frac{m_j}{\rho_j}\nabla^{(2)}W(\mathbf{r}_{ji})\mathbf{r}_{ji}^{\text{T}}\boldsymbol{M}_{1,\text{CSPM}}^{-1}\sum_{k=1}^{N}\frac{m_k}{\rho_k}(p_k-p_I)\nabla W(\mathbf{r}_{ji})\right) \quad (11)$$

in which $I_{\text{CSPM}} = [1 \quad 0 \quad 0 \quad 1 \quad 0 \quad 1]^{\text{T}}$; $\boldsymbol{M}_{1,\text{CSPM}} = \sum_{j=1}^{N}\frac{m_j}{\rho_j}\nabla W(\mathbf{r}_{ji})\mathbf{r}_{ji}^{\text{T}}$ is a 3×3 matrix for 3D problems or 2×2 matrix for 2D problems; $\boldsymbol{M}_{2,\text{CSPM}} = \sum_{j=1}^{N}\frac{m_j}{\rho_j}\nabla^{(2)}W(\mathbf{r}_{ji})\left(\boldsymbol{r}_{jI}^{(2)}\right)^{\text{T}}$ is the matrix with size of 6×6 for 3D problems or 3×3 for 2D problems and $\boldsymbol{r}_{ji}^{(2)} = \left[x_{ji}^2\ 2x_{ji}y_{ji}\ 2x_{ji}z_{ji}\ y_{ji}^2\ 2y_{ji}z_{ji}\ z_{ji}^2\right]^{\text{T}}$, $\boldsymbol{\nabla}^{(2)} = \left[\frac{\partial^2}{\partial x^2}\ \frac{\partial^2}{\partial x\partial y}\ \frac{\partial^2}{\partial x\partial z}\ \frac{\partial^2}{\partial y^2}\ \frac{\partial^2}{\partial y\partial z}\ \frac{\partial^2}{\partial z^2}\right]^{\text{T}}$. The other one is the CSPH2Γ scheme developed by Schwaiger (2008),

$$\nabla^2 P_i = 2\boldsymbol{I}^{\text{T}}\boldsymbol{M}_{2,\text{CSPH}}^{-1}\left(\sum_{j=1}^{N}\frac{m_j}{\rho_j}(P_j-P_I)\tilde{\nabla}W(\mathbf{r}_{ji}) - \sum_{j=1}^{N}\frac{m_j}{\rho_j}\boldsymbol{r}_{jI}^{\text{T}}\tilde{\nabla}W(\mathbf{r}_{ji})\nabla P_i\right) \quad (12)$$

where $\boldsymbol{M}_{2,\text{CSPH}} = \sum_{j=1}^{N}\frac{m_j}{\rho_j}\tilde{\nabla}W(\mathbf{r}_{ji})\left(\mathbf{r}_{ji}^{(2s)}\right)^{\text{T}}$ is a matrix with size of 3×3 for 3D problems or 2×2 for 2D problems, in which $\mathbf{r}_{ji}^{(2s)} = \left[x_{ji}^2 \quad y_{ji}^2 \quad z_{ji}^2\right]^{\text{T}}$ and $\tilde{\nabla}W(\mathbf{r}_{ji}) =$

Commented [YS17]: Reviewer 2: M8

Commented [ZN18]: Reviewer 2: Q7

Commented [ZN19]: Reviewer 2: M9

$\frac{1}{d_{ji}^2}\left[x_{ji}\frac{\partial W_{ji}}{\partial x} \quad y_{ji}\frac{\partial W_{ji}}{\partial y} \quad z_{ji}\frac{\partial W_{ji}}{\partial z}\right]^{\mathrm{T}}$ with $d_{ji} = |\mathbf{r}_{ji}|$. The pressure gradient in Eq. (12) is estimated using,

$$\nabla P_i = \boldsymbol{M}_{1,\mathrm{CSPM}}^{-1} \sum_{j=1}^{N} \frac{m_j}{\rho_j}\left(P_j - P_I\right)\nabla W\left(\mathbf{r}_{ji}\right) \tag{13}$$

A detailed error analysis of these two schemes has been given in Yan et al. (2020), which shows the leading truncation errors of the CSPM (Eq. (11)) and CSPH2Γ (Eq. (12)) for irregular particle distributions are termed by 2nd derivatives of the pressure and mainly sourced from the truncation error of the gradient estimation using Eq. (13).

3. Mathematical Formulation of QSFDI

The QSFDI is developed based on the principle of the SFDI to derive the interpolation, gradient estimation and Laplacian discretisation schemes with a quadric accuracy. It is derived by using Taylor's expansion. For each particle j at the location $\boldsymbol{x}_j$, which is inside the support domain of the particle i at $\boldsymbol{r}_i$, a function P can be expressed as the Taylor's expansion,

$$p_j - p_i = \mathbf{r}_{ji}^{\mathrm{T}}\nabla P_i + \frac{1}{2}\left(\mathbf{r}_{ji}^{(2s)}\right)^{\mathrm{T}}\nabla^{(2s)}P_i + \left(\boldsymbol{r}_{ji}^{(2c)}\right)^{\mathrm{T}}\nabla^{(2c)}P_i + \frac{1}{6}\left(\mathbf{r}_{ji}^{T}\nabla\right)^{3}P_i + \cdots \tag{14}$$

In Eq. (14), the 2nd-derivative term $\frac{1}{2}\left(\mathbf{r}_{ji}^{T}\nabla\right)^{2}P_i$ in the conventional Taylor's expansion (e.g., Chen *et al.*, 1999; Tamai, *et al.*, 2017) is split into two, i.e., $\frac{1}{2}\left(\mathbf{r}_{ji}^{(2s)}\right)^{\mathrm{T}}\nabla^{(2s)}P_i$ and $\left(\mathbf{r}_{ji}^{(2c)}\right)^{\mathrm{T}}\nabla^{(2c)}P_i$ where $\boldsymbol{r}_{jI}^{(2c)} = [x_{jI}y_{jI} \quad x_{jI}z_{jI} \quad y_{jI}z_{jI}]^{\mathrm{T}}$, $\boldsymbol{\nabla}^{(2s)} = \left[\frac{\partial^2}{\partial x^2} \quad \frac{\partial^2}{\partial y^2} \quad \frac{\partial^2}{\partial z^2}\right]^{\mathrm{T}}$ and $\boldsymbol{\nabla}^{(2c)} = \left[\frac{\partial^2}{\partial x\partial y} \quad \frac{\partial^2}{\partial x\partial z} \quad \frac{\partial^2}{\partial y\partial z}\right]^{\mathrm{T}}$.

Following Ma (2008), the weighted summation of Eq. (14) for all particles in the support domain of the particle i are used to derive the schemes for approximating the gradient∇P_i, 2nd derivatives and Laplacian$\boldsymbol{\nabla^2}P_i$, as well as the interpolation function for approximation P_i. Only the final formulas are summarised here and more details of the derivation can be found in Yan et al. (2020).

$$\nabla P_i = \sum_{j=1}^{N}\boldsymbol{\Phi}_{ji}^{g}\left(p_j - p_i\right) \tag{15}$$

$$\nabla^{\boldsymbol{2}}P_i = \boldsymbol{I}^{\mathrm{T}}\sum_{j=1}^{N}\boldsymbol{\Phi}_{ji}^{s}\left(p_j - p_i\right) \tag{16}$$

where $\boldsymbol{I} = [1 \quad 1 \quad 1]^{\mathrm{T}}$ and

$$\boldsymbol{\Phi}_{jI}^{g} = \boldsymbol{M}_{1q,i}^{-1}\left(\frac{W(\mathbf{r}_{ji})}{d_{ji}^2}\boldsymbol{q}_{ji} - \sum_{k=1}^{N}\frac{W(\mathbf{r}_{ki})}{d_{ki}^2}\boldsymbol{q}_{ki}\left(\mathbf{r}_{ki}^{(2c)}\right)^{\mathrm{T}}\boldsymbol{M}_{2c,i}^{-1}\frac{W(\mathbf{r}_{ji})}{d_{ji}^4}\mathbf{r}_{jI}^{(2c)} - \sum_{k=1}^{N}\frac{w_{kI}}{d_{ki}^2}\boldsymbol{q}_{ki}\boldsymbol{\Pi}_{ki}^{\mathrm{T}}\boldsymbol{M}_{2s,i}^{-1}\boldsymbol{\Gamma}_{ji}\right) \tag{17}$$

$$\boldsymbol{\Phi}_{ji}^{s} = 2\boldsymbol{M}_{2s,i}^{-1}\left(\boldsymbol{\Gamma}_{ji} - \sum_{k=1}^{N}\frac{w_{kI}}{d_{ki}^{4}}\boldsymbol{\Pi}_{ki}\boldsymbol{G}_{ki}^{\mathrm{T}}\boldsymbol{\Phi}_{ki}^{g}\right) \tag{18}$$

Definitions of matrices in Eq. (17) and (18) are as follows

$$\boldsymbol{M}_{2c,i} = \sum_{j=1}^{N}\frac{W(\mathbf{r}_{ji})}{d_{ji}^{4}}\mathbf{r}_{ji}^{(2c)}\left(\mathbf{r}_{ji}^{(2c)}\right)^{\mathrm{T}},$$

$$\boldsymbol{\Pi}_{ji} = \left\{\left(\mathbf{r}_{ji}^{(2s)}\right)^{\mathrm{T}} - \left(\mathbf{r}_{ji}^{(2c)}\right)^{\mathrm{T}}\boldsymbol{M}_{2c,i}^{-1}\sum_{k=1}^{N}\frac{W(\mathbf{r}_{ki})}{d_{ki}^{4}}\mathbf{r}_{ki}^{(2c)}\left(\mathbf{r}_{ji}^{(2s)}\right)^{\mathrm{T}}\right\}^{\mathrm{T}},$$

$$\boldsymbol{M}_{2s,i} = \sum_{j=1}^{N}\frac{W(\mathbf{r}_{ji})}{d_{ji}^{4}}\boldsymbol{\Pi}_{jI}\boldsymbol{\Pi}_{jI}^{\mathrm{T}}$$

$$\boldsymbol{G}_{ji} = \left\{\mathbf{r}_{ji}^{\mathrm{T}} - \left(\mathbf{r}_{ji}^{(2c)}\right)^{\mathrm{T}}\boldsymbol{M}_{2c,i}^{-1}\sum_{k=1}^{N}\frac{W(\mathbf{r}_{ki})}{d_{ki}^{4}}\mathbf{r}_{ki}^{(2c)}\mathbf{r}_{ki}^{T}\right\}^{\mathrm{T}},$$

$$\boldsymbol{F}_{ji} = \left\{\left(\mathbf{r}_{ji}^{(3)}\right)^{\mathrm{T}} - \left(\mathbf{r}_{ji}^{(2c)}\right)^{\mathrm{T}}\boldsymbol{M}_{2c,I}^{-1}\sum_{k=1}^{N}\frac{W(\mathbf{r}_{ki})}{d_{ki}^{4}}\mathbf{r}_{ki}^{(2c)}\left(\mathbf{r}_{ki}^{(3)}\right)^{\mathrm{T}}\right\}^{\mathrm{T}},$$

$$\boldsymbol{q}_{ji} = \left(\boldsymbol{G}_{ji}^{T} - \boldsymbol{\Pi}_{ji}^{\mathrm{T}}\boldsymbol{M}_{2s,I}^{-1}\sum_{k=1}^{N}\frac{W(\mathbf{r}_{ki})}{d_{ki}^{4}}\boldsymbol{\Pi}_{ki}\boldsymbol{G}_{ki}^{\mathrm{T}}\right)^{\mathrm{T}},$$

$$\boldsymbol{\Gamma}_{ji} = \left(\frac{W(\mathbf{r}_{ji})}{d_{ji}^{4}}\boldsymbol{\Pi}_{ji} - \boldsymbol{\Pi}_{ji}\left(\mathbf{r}_{ji}^{(2c)}\right)^{\mathrm{T}}\boldsymbol{M}_{2c,I}^{-1}\sum_{k=1}^{N}\frac{w_{ki}}{d_{ki}^{4}}\mathbf{r}_{ki}^{(2c)}\right),$$

$$\boldsymbol{M}_{1q,i} = \sum_{j=1}^{N}\frac{W(\mathbf{r}_{ji})}{d_{ji}^{2}}\boldsymbol{q}_{ji}\boldsymbol{q}_{ji}^{\mathrm{T}},$$

where $\mathbf{r}_{ji}^{3} = [x_{ji}^{3}\ \ 3x_{ji}^{2}y_{ji}\ \ 3x_{ji}^{2}z_{ji}\ \ 3x_{ji}y_{ji}^{2}\ \ 6x_{ji}y_{ji}z_{ji}\ \ 3x_{ji}z_{ji}^{2}\ \ y_{ji}^{3}\ \ 3y_{ji}^{2}z_{ji}\ \ 3y_{ji}z_{ji}^{2}\ \ z_{ji}^{3}]^{\mathrm{T}}$.

Error analysis of the QSFDI by Yan et al. (2020) shows that the leading truncation errors of Eq. (15) and Eq. (16) are termed by the third derivative of *P*. Theoratically, the QSFDI has better accuracy and convergence properties than the CSPM and the CSPH2Γ. This has been confirmed by the patch test conducted by Yan et al. (2020), in which various mathematical functions, including exponential and trigonometric functions, have been considered; QSFDI, CSPM, CSPH2Γ and other schemes have been used to directly estimate the Laplacian of these functions or to solve the Poisson equations formulated by these functions in a truncated domain discretised by randomly distributed particles (reflecting the feature of the particle distribution in ISPH application). The results suggested that the QSFDI requires considerably less computational time to achieve the same accuracy compared with other schemes used in the patch tests; and it results in a quadric convergent rate for solving Poisson equations, which is one-order higher than the CSPM and CSPH2Γ. Nevertheless, whether the QSFDI would deliver promising feature during the real applications as the patch tests remains unknown. This will be demonstrated in the following comparative study.

4. Comparative Study on Wave Propagation and Impact on Structures

Tab.1 Summary of different ISPH numerical schemes

Commented [YS20]: Reviewer 2: M11

Commented [ZN21]: Reviewer 2: Q8
Handling Editor: Q3

Schemes	Formulations	
ISPH	$\nabla\cdot\left(\frac{1}{\rho}\nabla P_i\right)=\sum_{j=1}^{N}\frac{8m_j}{(\rho_i+\rho_j)^2}\frac{(P_i-P_j)\mathbf{r}_{ij}}{r_{ij}^2+\eta^2}\cdot\nabla_i W(\mathbf{r}_{ij})$	Eq. (10)
ISPH_CSPM	$\nabla^2 P_i=2\boldsymbol{I}_{\mathrm{CSPM}}^{\mathrm{T}}\boldsymbol{M}_{2,\mathrm{CSPM}}^{-1}\left(\sum_{j=1}^{N}\frac{m_j}{\rho_j}(P_j-P_I)\nabla^{(2)}W(\mathbf{r}_{ji})-\sum_{j=1}^{N}\frac{m_j}{\rho_j}\nabla^{(2)}W(\mathbf{r}_{ji})\mathbf{r}_{ji}^{\mathrm{T}}\boldsymbol{M}_{1,\mathrm{CSPM}}^{-1}\sum_{k=1}^{N}\frac{m_k}{\rho_k}(p_k-p_I)\nabla W(\mathbf{r}_{ji})\right)$	Eq. (11)
ISPH_CSPH2Γ	$\nabla^2 P_i=2\boldsymbol{I}^{\mathrm{T}}\boldsymbol{M}_{2,\mathrm{CSPH}}^{-1}\left(\sum_{j=1}^{N}\frac{m_j}{\rho_j}(P_j-P_I)\tilde{\nabla}W(\mathbf{r}_{ji})-\sum_{j=1}^{N}\frac{m_j}{\rho_j}\mathbf{r}_{ji}^{\mathrm{T}}\tilde{\nabla}W(\mathbf{r}_{ji})\nabla P_i\right)$ $\nabla P_i=\boldsymbol{M}_{1,\mathrm{CSPM}}^{-1}\sum_{j=1}^{N}\frac{m_j}{\rho_j}(P_j-P_I)\nabla W(\mathbf{r}_{ji})$	Eq. (12,13)
ISPH_QSFDI	$\nabla^2 P_i=\boldsymbol{I}^{\mathrm{T}}\sum_{j=1}^{N}\boldsymbol{\Phi}_{ji}^{s}(p_j-p_i)$	Eq. (16)

In this section, the numerical comparative study on modelling the wave-structure interactions is conducted. It considers various cases including the solitary wave propagation, the wave impact on vertical and inclined walls, and the evolution of focusing waves. The performance of the QSFDI (Eq. (16)) for discretising the Laplacian operator in the PPE (Eq. (3)) is examined. For the purpose of comparison, other Laplacian discretisation schemes, including the CSPM (Eq. (11)), CSPH2Γ (Eq. (12)) and the scheme commonly used by ISPH (Eq. (10)), are also used. For clarity, these schemes are referred to as the ISPH_QSFDI, ISPH_CSPM, ISPH_ CSPH2Γ and ISPH, respectively, as summarised in Table 1.

As indicated above, the leading truncation error of Laplacian discretisation in the QSFDI is termed by the third derivatives of pressure, which is one order higher than the CSPM and CSPH2Γ. However, in addition to the Laplacian discretization, the accuracy and convergence of solving the PPE also depends on the estimation of its right-hand side, the implementation of the numerical schemes to deal with the boundary conditions on the free surface and solid boundaries, and the solver for solving the linear algebraic equations resulting from the discretized PPE. In this paper, we mainly focus our attention to the performances of different Laplacian discretisation schemes, other numerical implementations are taken as the same for different ISPH schemes considered in the comparative study. These include a linear scheme (Eq. (7)) for estimating the velocity divergence in the right-hand side of the PPE, a linear scheme (Eq. (9)) for gradient estimation and implementing the solid-boundary condition. These match the accuracies of the Laplacian discretisation in the classic ISPH, ISPH _CSPM and ISPH _CSPH2Γ but would downgrade the overall accuracy of solving the PPE in the ISPH_QSFDI. Furthermore, the overall accuracy of the projection-based ISPH is

also influenced by the estimations of the pressure gradient, viscous stress and velocity divergence, e.g. Eqs. (7-9), the time integration schemes for updating the velocity and displacement of the Lagrangian particles, the particle stabilization scheme. For the same reason, their numerical implementations remain the same for different ISPH schemes listed in Table 1. For convenience, the implementations commonly applied by different ISPH schemes are summarised in Table 2.

Table 2: Numerical implementations of ISPH schemes

	Scheme/model
Velocity divergence	Eq. (7)
Viscous stress	Eq. (8)
Pressure gradient	Eq. (9)
Intermediate velocity, density	$\mathbf{u}^* = \mathbf{u}^t + (\mathbf{g} + \nu\nabla^2\mathbf{u})^t\Delta t$ where the viscous term is estimated using Eq. (8) ; $\rho^* = \sum_{j=1}^{N} m_j W(\mathbf{r}_{ij})$
Linear algebraic solver	Bi-CGSTAB method (Van der Vorst, 1992) without pre-conditioning. Tolerance 10^{-5}.
Free surface condition	Eq. (6), free surface particle is identified by using a method based on the auxiliary functions (Zheng, et al, 2014)
Solid boundary condition	Similar to Lo and Shao (2002), the solid boundaries are simulated by particles with mirror particles placed outside the solid walls. Eq. (5) is, directly discretized by using the SFDI (Ma and Zhou, 2009, Zheng, et al, 2014)
Kernel funciton	cubic B-spline kernel proposed by Monaghan and Lattanzio (1985)
Particle stabilization	The hybrid particle stabilization scheme proposed by Zhang et al., (2018)

Commented [YS22]: Reviewer 2: Q 10

4.1. Solitary wave propagation and impact on a vertical wall

The first case considered here is the solitary wave impact on a vertical wall. The experiment was carried out by Zheng et al. (2015) in a 3-D wave flume with a piston wavemaker in the Harbin Engineering University (HEU). The schematic diagram of the wave tank is shown in **Fig. 1.** The solitary wave height is h = 0.15 m and the water depth d is 0.25 m, yielding a wave nonlinearity $\varepsilon = h/d$ of 0.6. A pressure sensor P_1 is placed on the right end of the tank with a distance of 0.05 m above the tank bottom. The length of the wave tank L is 10 m. In the numerical investigation, different particle spacing is used to evaluate the convergence rate of different ISPH schemes.

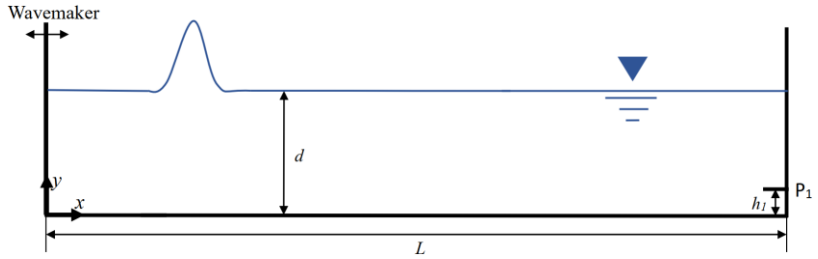

Fig. 1 Schematic wave tank for solitary wave impact on a vertical wall

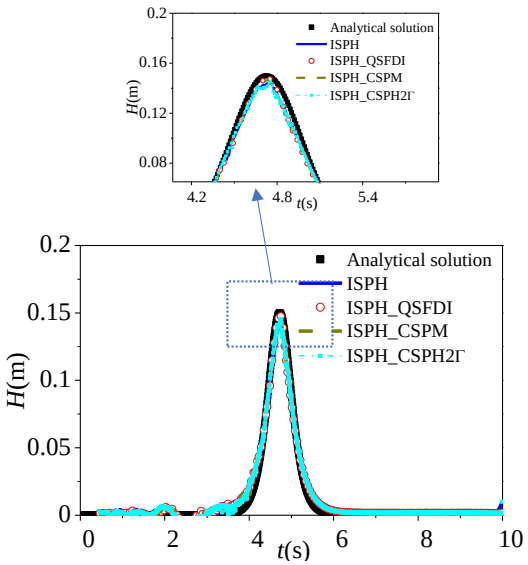

Fig. 2 Comparisons of wave surface profiles between analytical solution and different ISPH results at t = 3.1 s

Fig. 2 compares the free surface profiles at t = 3.1 s obtained by different schemes with the same particle spacing dx of 0.01m (the corresponding number of particle N = 25,000) and the analytical solution from the Boussinesq equation (Lee et al., 1982). One may observe that all ISPH schemes lead to satisfactory results with reference to the analytical solution; there are differences in the wave crest and the ISPH_QSFDI results in better accuracy in the free surface profiles compared with other schemes. It is clearer in the error analysis illustrated in Fig. 3.

Commented [ZN23]: Handling Editor: Q4

Commented [ZN24]: Reviewer 2: M12

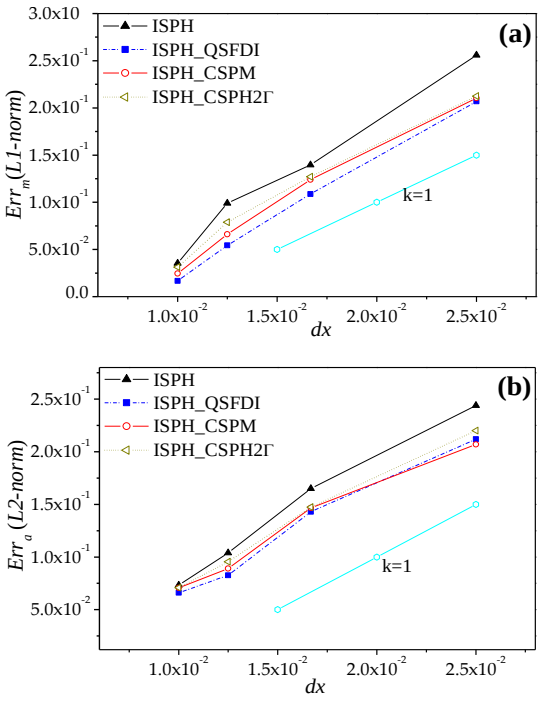

Fig. 3. Errors of numerical results corresponding to different numbers of particles.

Commented [ZN25]: Reviewer 2: Q15

Fig. 3 compares the relative errors Err_m (L1-norm) in terms of the maximum wave elevations ζ_{max}**(Fig. 3(a))** and the averaged errors on the wave surface profiles Err_a (L2-norm) **(Fig. 3(b))** of the ISPH results in the cases with different particle spacing. Err_m (L1-norm) is defined by $Err_m = |\zeta^a_{max} - \zeta^n_{max}|/\zeta^a_{max}$, where the superscripts a and n denote the analytical and numerical results, respectively. Err_a (L2-norm) is defined by $Err_a = \frac{\sqrt{\sum_{i=1}^{N}(\zeta_i^a - \zeta_i^n)^2}}{\sqrt{\sum_{i=1}^{N}(\zeta_i^a)^2}}$, where ζ_i is the wave elevations recorded at ??? at different time steps and N is the total number of time steps in the duration from t = 4 s to t = 5.4 s. For convenience, a straight line representing the linear convergence rate k=1 is included. Consistent with the patch test by Yan et al. (2020), the ISPH _CSPM and ISPH _CSPH2Γ exhibit a linear rate of reduction of the error as the particle size decreases (linear convergence rate), so does the classic ISPH. However, the ISPH_QSFDI showed a quadric convergence rate in the patch test by Yan et al. (2020) but a linear convergence rate in Fig. 3. The main reason is that the right-hand side of the Poisson equation is given by the exact value formulated by given function in Yan

et al. (2020), whereas in the present work, the right-hand side of the PPE is evaluated by a linear scheme (Eq. 7) . Furthermore, the patch test in Yan et al (2020) was conducted in a truncated domain with exact solutions providing on the boundaries, whereas a linear scheme (Eq. (9)) is used to impose the solid boundary condition. This confirms our analysis stated above regarding the reduction of the accuracy of the QSFDI by these linear schemes. Nevertheless, it is observed from Fig. 3 that the relative error of the present ISPH_QSFDI is lower than other schemes with different numbers of particles, implying that the present ISPH_QSFDI is more accurate than other schemes if the same particle spacing is considered.

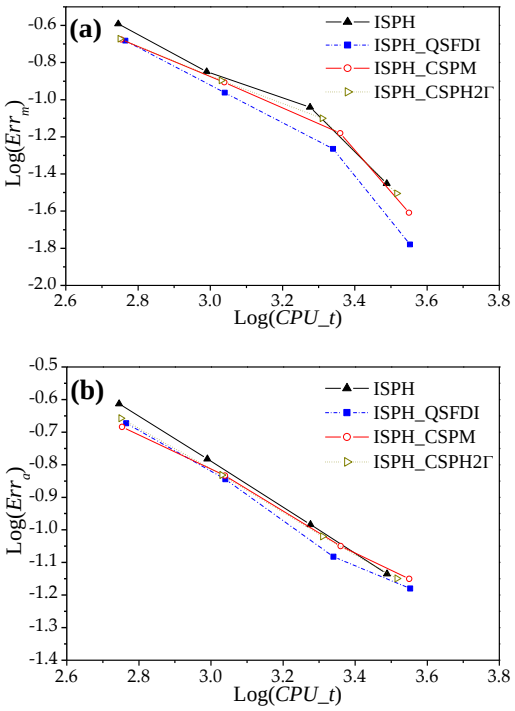

Fig. 4. CPU times corresponding to different errors.

In order to compare the robustness of the schemes, the CPU time spent by all the schemes corresponding to different numerical errors are illustrated in **Fig. 4**, which clearly shows that the ISPH_ QSFDI requires shorter CPU time to achieve the same level accuracy than other schemes, especially, in terms of the Err_m (L1-norm) corresponding to the maximum wave elevation, which is of great concern in

engineering practices.

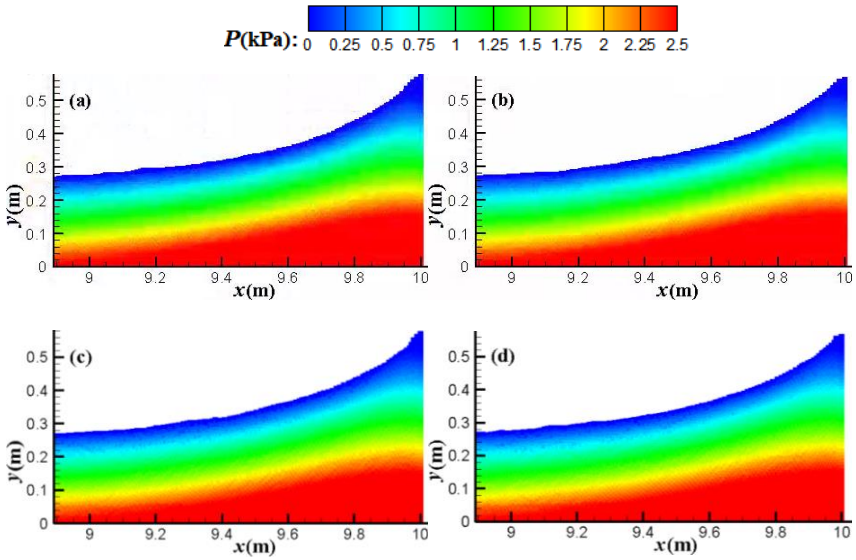

Fig. 5 The particle distributions with pressure contour: (a) standard ISPH; (b) ISPH_QSFDI; (c) ISPH_CSPM; and (d) ISPH_CSPH2Γ

Fig. 5 illustrates the particle distributions with pressure contour from the classic ISPH (Shao and Lo, 2003) and other ISPH schemes at the time instant corresponding to the highest elevation on the right end of the tank. In these case, N = 25000 and dx = 0.01 m. It seems that all schemes yield an appropriate and smooth pressure field. The corresponding quantitative comparison of the impact pressure at the sensor point P_1 is shown in **Fig. 6**. Satisfactory agreements between the numerical results and the experimental data are observed by all ISPH schemes. To demonstrate the convergence properties, the error of the pressure predictions in the cases with different particle spacing is analyzed and **Fig. 7** displays the averaged errors (L2-norm) of the pressure during t = 5.7 s to t = 6.1 s. Similar to Fig.3, **Fig. 7** evidences that the ISPH_QSFDI achieves better accuracy than other schemes except in the case with the coarsest particle resolution.

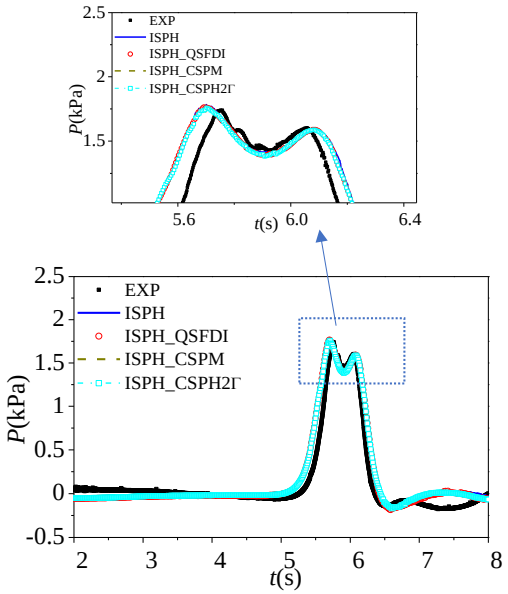

Fig. 6 Comparisons of wave impact pressures between experimental data and different ISPH results

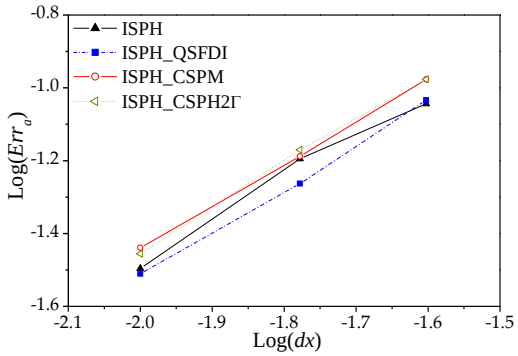

Fig. 7 Errors of the impact pressure of four numerical methods corresponding to different numbers of particles.

For wave propagations, the energy conservation is a critical problem. The energy conservations in results predicted by different schemes are examined. **Fig. 8** shows the time histories of the total energy of the fluid in the wave tank for solitary wave propagating in wave tank with L = 40 m, where wave condition is the same as the cases presented above and the particle spacing is ???. As shown, the total energy increases up to t = 1.5 s (???) when the wavemaker stops. During this period, the fluid in the wave

tank acquires the energy from the wavemaker. After that, all numerical results exhibit energy loss. The rate of the reduction becomes relatively steady after t = 15 s. It can be seen that the present ISPH_QSFDI schemes has better energy conservation performance than other schemes for solitary wave propagation.

Commented [ZN26]: Reviewer 1: Q5

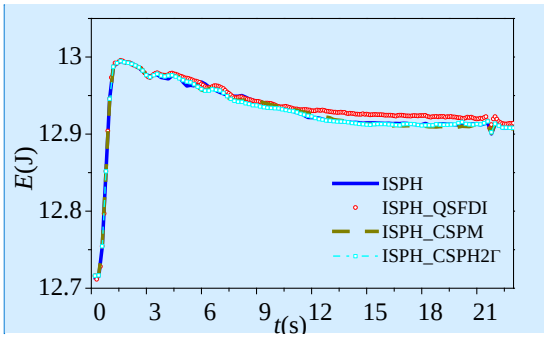

Fig. 8. Time history of the energy changes of different ISPH schemes.

Commented [YS27]: Ningbo, Can you make the y-axis ranged from 12.9 to 13? We need to highlight it
总能量减去初始时刻的能量

4.2. Solitary wave overtopping on an impermeable seawall

The second case considered here is the solitary wave impact on an impermeable trapezoidal seawall. The experiment was carried out by Hsiao and Lin (2010) and the corresponding experimental data was extracted from the publication to evaluate the performances of all ISPH schemes. For clarity, the relevant parameters as that in experiment are sketched in **Fig. 9**. For the analysis of numerical results, the relative time $t' = t - t_{MR}$ is used, where t_{MR} corresponds to the instant when the wave run-up at the wall reaches the maximum value. The solitary wave is generated by a wavemaker. The numerical simulations are carried out to achieve 10-second results of the wave propagation and interacting with the sea wall. The wave gauge "*G*" and pressure probe "*P*" are also illustrated in **Fig. 9**.

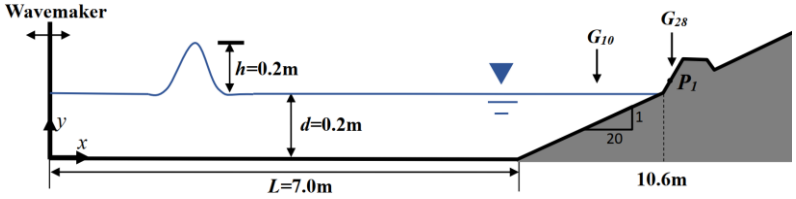

Fig. 9 Schematic setup of wave tank for solitary wave impact and overtopping.

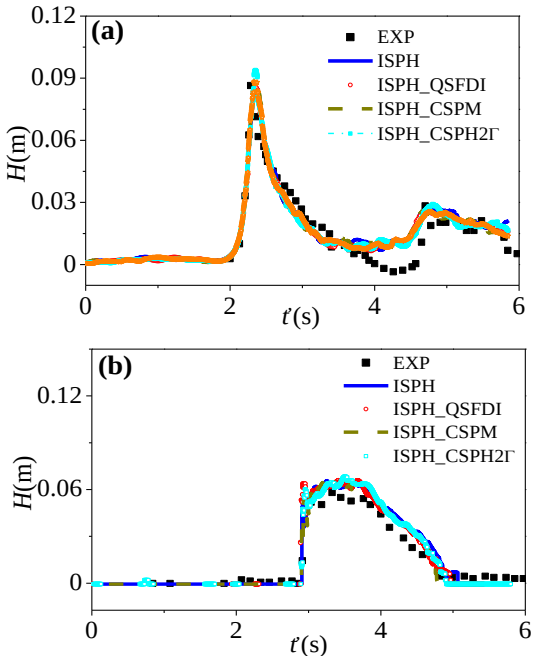

Fig. 10 Wave time history recorded at (a) G_{10} (x = 9.644 m) and (b) G_{28} (x = 10.732 m) (experimental data is supplicated from Hsiao and Lin, 2010)

Commented [ZN28]: Reviewer 2: Q20

Fig. 10 compares the wave time histories recorded at G_{10} and G_{28} which are located at 9.644 m and 10.732 m from the initial position of the wavemaker. For the purpose of comparison, the experimental data by Hsiao and Lin (2010) is plotted together. In these cases, the particle spacing dx is taken as 0.01m. As observed, all numerical schemes lead to acceptable results. Due to the fact that the experimental data were extracted from the publication and therefore may not be sufficiently accurate to be the reference value when evaluating the quantitative error, the numerical results with the finest particle resolutions, i.e. dx = 0.01, is used to evaluate the errors of results with lower-resolution particles. The averaged errors of different methods are obtained by $Err_a = \frac{\sqrt{\sum_{i=1}^{N}\left(\zeta_i^f-\zeta_i^n\right)^2}}{\sqrt{\sum_{i=1}^{N}\left(\zeta_i^f\right)^2}}$, where the superscript f denotes the results from the simulation with finesse particle resolution.

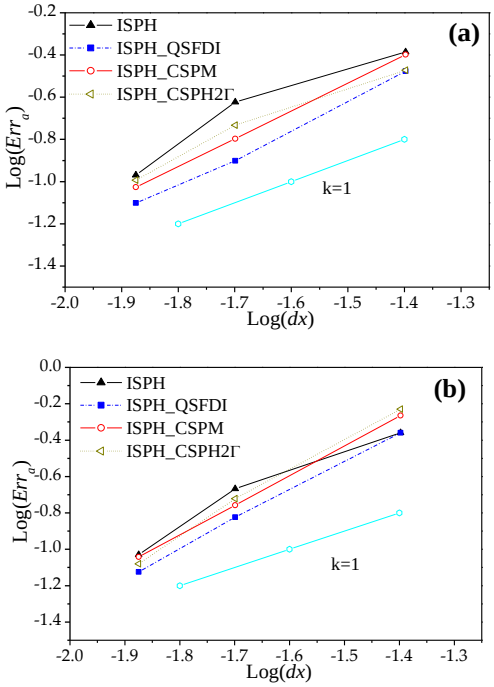

Fig. 11. Errors of ISPH schemes in the cases with different numbers of particles at (a) G_{10} (x = 9.644 m) and (b) G_{28} (x = 10.732 m)

Fig. 11 illustrates the averaged errors with reference to the rsults shown in **Fig. 10** using the durations of t = 2 – 4 s for (a) and t = 3 - 5 s for (b), respectively. The corresponding results on the CPU time are shown in **Fig. 12**. Overally, the ISPH_QSFDI has a similar convergence property to other schemes, but results in a higher accuracy for specific particle spacing than other schemes. More importantly, the CPU time required by the ISPH_QSFDI to achieve a specific accuracy is generally shorter than other schemes.

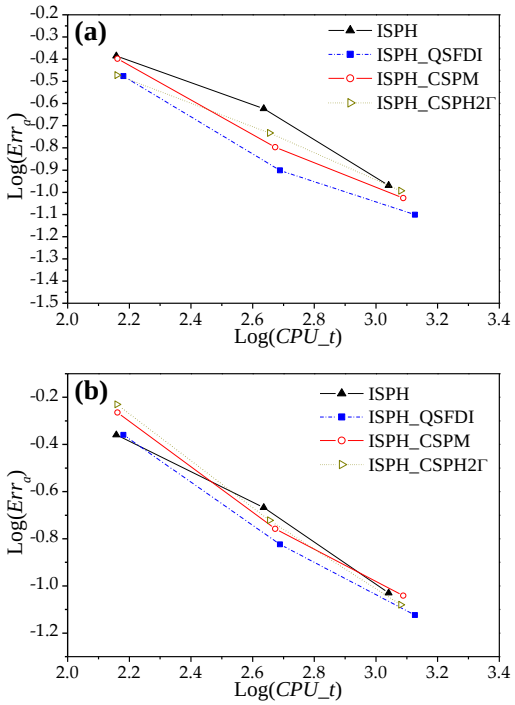

Fig. 12. CPU times corresponding to different errors at: (a) G_{10}; (b) G_{28}.

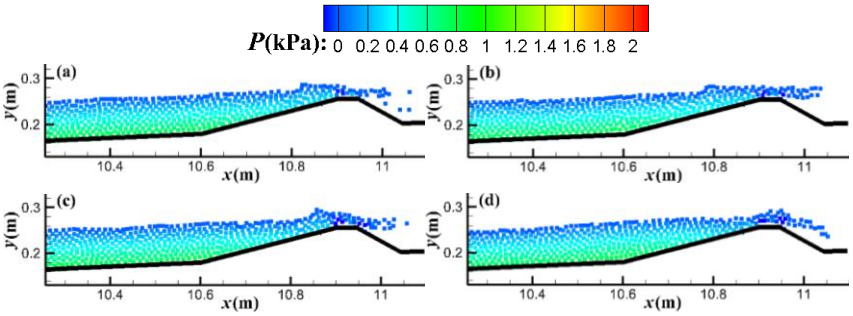

Fig. 13 Particle distributions with contour of pressures near the sea wall for (a) standard ISPH; (b) ISPH_QSFDI; (c) ISPH_CSPM; and (d) ISPH_CSPH2Γ

Fig. 13 shows snapshots of particles with contour of the pressure field during the wave impinging and overtopping on the trapezoidal caisson. As the wave overtops over the seawall, an overtopping tongue develops on the crown. One may see an obvious differences in the shape of the tongue and the free surface near the wall. All schemes

Commented [ZN29]: Handling Editor: Q2

seem to deliver smooth pressure field in Fig. 13.

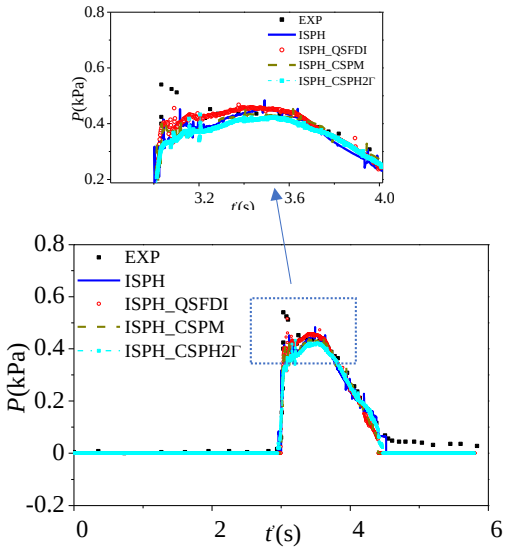

Fig. 14 Comparisons of wave impact pressures between experimental data and different ISPH results

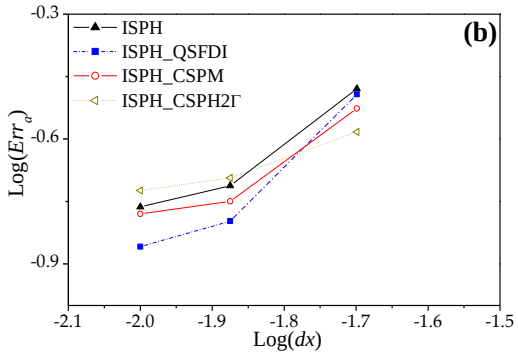

Fig. 15 Comparisons of average errors of the impact pressure of four numerical methods corresponding to different support size.

Furthermore, **Fig. 14** compares the impact pressures computed by using different ISPH schemes recorded by the pressure sensor P_1 at coordinate (10.83, 0.249) on the trapezoidal structure. It is shown that the general trends of impact pressures computed by all ISPH schemes show a good consistency with the experimental data, although

there are some discrepancies due to the complication of the physical problem. **Fig. 15** shows the averaged errors of the pressure during t =3.0 s to t =4.3 s in the cases with different particle spacing. Once again, similar conclusion can be drawn for the improvement in the accuracy and convergence by the QSFDI compared with other schemes.

Commented [ZN30]: Reviewer 1: Q6

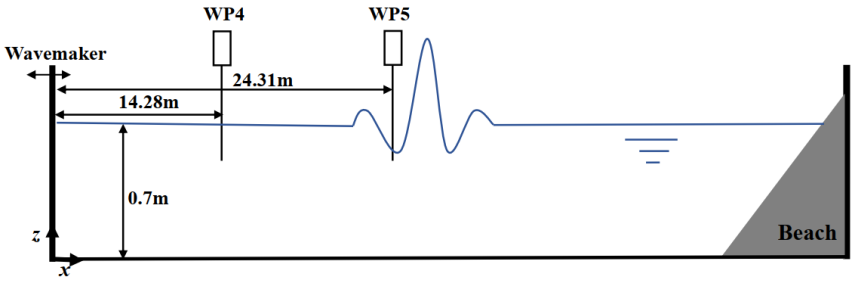

Fig. 16. Sketch of the experimental setup

4.3. Focusing wave propagation

The last case considered in this paper is the focusing wave propagation. Compared with the solitary waves, which were taken into account in the above two cases, the focusing wave is more popularly used in the offshore engineering to represent the extreme waves. It typically consists of a list of wave components with a wide frequency range and is generally generated using spatial-temporal focusing mechanism in the laboratory. In this paper, the experiments conducted by Sriram et al. (2015) at the Ludwig-Franzius-Institute at Leibniz University of Hannover, Germany are considered as the reference values. As sketched in **Fig. 16**, the tank has a working depth of 0.7 m. The focused waves are generated by using the second-order wavemaker theory, as described in Sriram et al. (2015) and Sriram et al. (2020). In the experiments, wave probes WP4 and WP5 will be used to validate the focused wave generation and propagation.

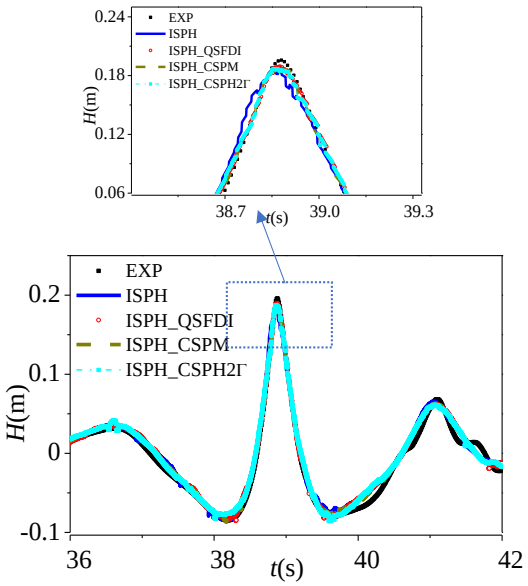

Fig. 17. Wave time histories of focusing waves (experimental data obtained from Sriram et al., 2020)

Fig. 17 compares the wave time histories recorded at WP5 in which a focused wave height of 0.3 m is generated using a constant steepness spectrum of 32 components ranging from 0.34 to 1.02 Hz (Sriram et al., 2015). The particle spacing dx = 0.01 m is used by all ISPH schemes and results in a satisfactory agreement between the experimental data and any sets of the numerical results. As an essential practice, the convergence properties of these methods are examined in terms of the wave surface elevations at the wave probes WP5 from 38.2 s to 39.6 s (**Fig. 17**). The results are displayed in Fig. 18, from which one can find that the averaged error of the ISPH_QSFDI and ISPH_CSPM decrease as the particle spacing dx decreases at a nearly linear rate, whereas the ISPH and ISPH_CSPH2Γ converge at a rate lower than a linear rate. This also provides evidence of the convergence of numerical results in spatial domains. Again, **Fig. 18** shows that the result of the ISPH_QSFDI method gives better agreement with experimental data than those of ISPH, ISPH_CSPM and ISPH_CSPH2Γ. To further evaluate the performance of the present model for the case considered here, the comparisons of the corresponding CPU time are also given in **Fig. 19**. These cases are run in parallel in OpenMP using 16 cores on a workstation with Intel i7 3.3 GHz and 128 GB RAM to achieve the results in a time window to 42.0 s. **Fig. 19** confirms the superiority of the ISPH_QSFDI in terms of saving CPU time for the same level of accuarrcy.

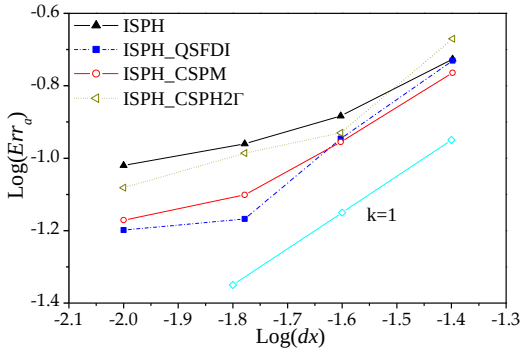

Fig. 18. Errors of numerical results from these numerical methods corresponding to different numbers of particles.

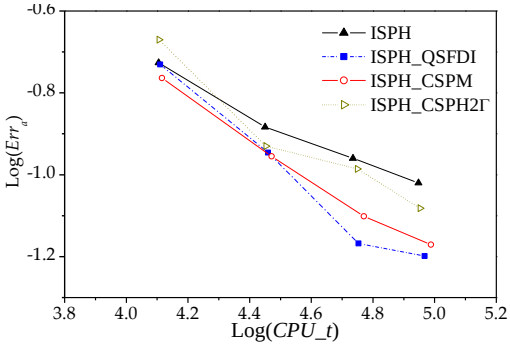

Fig. 19. CPU times spent by different numerical methods corresponding to different errors.

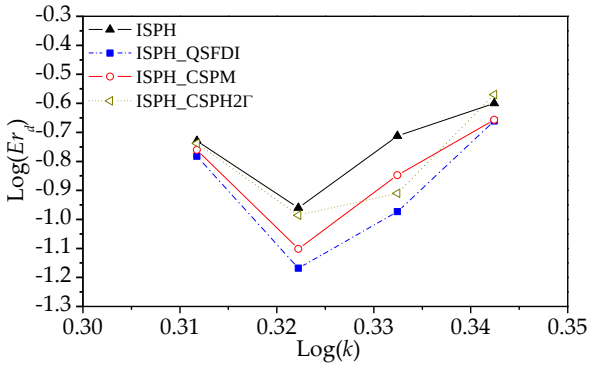

Fig. 20. Errors of numerical results with different support domain radius.

It is well recognised that the accuracy and convergence of the ISPH may be largely influenced by the support domain size. To shed light on this issue, different support domain sizes (support domain radius $r = k\mathrm{d}x$) are used by all ISPH schemes. Some results are shown in **Fig. 20**. It can be found that there is an optimised value of k, i.e. ???, results in a best accuracy for all schemes. No surprisedly, the ISPH_QSFDI schemes yields the best performance regardless the size of the support domain in these four methods.

5. Conclusions and Discussions

In this paper, the QSFDI is employed by the ISPH to discretise the Laplacian operator in the PPE. Its performance in modelling wave propagation and wave-structure interaction is assessed and compared with other schemes, including the classic ISPH, the CSPM and CSPH2Γ. This the first time, the QSFDI is extended to the practical application of the ISPH, following a systematic patch test in Yan et al . (2020).

For the emphasis in Laplacian discretisation, all other numerical implementations applied by different ISPH schemes are kept the same, despite the fact that such implementation would downgrade the overall accuracy of the QSFDI-based ISPH. It is found that the ISPH_QSFDI scheme generally has a better accuarcy than other schemes if the same number of particles in all the cases considered in the present investigation. It is also observed that the ISPH_QSFDI scheme requires considerably less computational time than other schemes to achieve the same accuracy.

However, the theritical quadric rate of the convergence of the QSFDI, which has been proved in the patch test (Yan et al. (2020)), was not observed in this investigation, due to the fact that the linear schemes are employed for estimating the right-hand side of the PPE and to deal with the boundary condition. In future, the ISPH_QSFDI scheme can be extended by using the QSFDI to deal with numerical interpolaiton and gradient estimation, yielding a quadric ISPH scheme with linear consistancy in solving the PPE.

Acknowledgement

The authors at City, University of London gratefully acknowledge the financial support of EPSRC projects (EP/T026782, EP/T00424X and EP/V040235). The author at Harbin Engineering University gratefully acknowledges the financial support by the National Natural Science Foundation of China (Grants 51879051, 51739001, 51579056, and 51639004).

References

Antuono, M., Colagrossi, A., Marrone, S., Molteni, D. (2010). Freesurface flows solved by means of sph schemes with numerical diffusive terms. Comput. Phys. commun. 181(3), 532-549.

Brookshaw, L. (1985). A method of calculating radiative heat diffusion in particle simulations. Publications of the Astronomical Society of Australia, 6(2), 207-210.

Chen J. K., Beraun J. E., Carney T. C. (1999). A corrective smoothed particle method for boundary value problems in heat conduction. International Journal for Numerical Methods in Engineering, 46(2), 231-252.

Cleary, P. W., Monaghan, J. J. (1999). Conduction modelling using smoothed particle hydrodynamics. Journal of Computational Physics, 148(1), 227-264.

Cummins, S. J., Rudman, M. (1999). An SPH projection method. Journal of Computational Physics, 152(2), 584-607.

Fatehi, R., Manzari, M. T. (2011). Error estimation in smoothed particle hydrodynamics and a new scheme for second derivatives. Computers & Mathematics with Applications, 61(2), 482-498.

Fourtakas, G., Stansby, P. K., Rogers, B. D., Lind, S. J. (2017). An Eulerian-Lagrangian incompressible SPH formulation (ELI-SPH) connected with a sharp interface. Computer Methods in Applied Mechanics & Engineering, S0045782517302050.

Fourtakas, G., Rogers, B. D., Nasar, A. (2021). Towards pseudo-spectral incompressible smoothed particle hydrodynamics (isph). Computer Physics Communications, 108028.

Gingold, R. A., Monaghan, J. J. (1977). Smoothed particle hydrodynamics - theory and application to non-spherical stars. Monthly Notices of the Royal Astronomical Society, 181(3), 375-389.

Gotoh, H., Khayyer, A. (2016). Current achievements and future perpectives for projection-based particle methods with applications in ocean engineering. Journal of Ocean Engineering and Marine Energy, 2(3), 251-278.

Gui, Q. Q., Dong, P., Shao, S. D., Chen, Y. Q. (2015). Incompressible sph simulation of wave interaction with porous structure. Ocean Engineering, 110, 126-139.

Hu, X. Y., Adams, N. A. (2007). An incompressible multi-phase SPH method. Journal of Computational Physics, 227(1), 264-278.

Hsiao, S. C., Lin, T. C. (2010). Tsunami-like solitary waves impinging and overtopping an impermeable seawall: experiment and RANS modeling. Coastal Engineering, 57(1), 1-18.

Inutsuka, S. I. (2002). Reformulation of smoothed particle hydrodynamics with riemann solver. Journal of Computational Physics, 179(1), 238-267.

Khayyer A., Gotoh H. (2012). A 3D higher order Laplacian model for enhancement and stabilization of pressure calculation in 3D MPS-based simulations. Applied Ocean Research, 37, 120-126.

Khayyer, A., Gotoh, H., Shimizu, Y., Gotoh, K. (2017a). On enhancement of energy conservation properties of projection-based particle methods. European Journal of Mechanics - B/Fluids, S0997754616302175.

Khayyer, A., Gotoh, H., Shimizu, Y. (2017b). Comparative study on accuracy and conservation properties of two particle regularization schemes and proposal of an optimized particle shifting scheme in ISPH context. Journal of Computational Physics, 332(1), 236-256.

Khayyer, A., Gotoh, H., Falahaty, H., Shimizu, Y. (2018). An enhanced ISPH-SPH coupled method for simulation of incompressible fluid-elastic structure interactions. Computer Physics Communications, 232, 139-164.

Khayyer, A., Shimizu, Y., Gotoh, H., Nagashima, K. (2021). A coupled incompressible SPH-Hamiltonian SPH solver for hydroelastic FSI corresponding to composite structures. Applied Mathematical Modelling, 94(1).

Lee, J. J., Skjelbreia, J. E., Raichlen, F. (1982). Measurement of velocities in solitary waves. Journal of the Waterway, 108(2), 200-218.

Lee, E. S., Moulinec, C., Xu, R., Violeau, D., Laurence, D., Stansby, P. (2008). Comparisons of weakly compressible and truly incompressible algorithms for the SPH mesh free particle method. Journal of Computational Physics, 227(18), 8417-8436.

Liang, D. F., Wei, J., Shao, S. D., Chen R. D., Yang, K. J. (2017). Incompressible sph simulation of solitary wave interaction with movable seawalls. Journal of Fluids and Structures, 69, 72-88.

Lind, S. J., Xu, R., Stansby, P. K., Rogers, B. D. (2012). Incompressible smoothed particle hydrodynamics for free-surface flows: a generalised diffusion-based algorithm for stability and validations for impulsive flows and propagating waves. Journal of Computational Physics, 231(4), 1499-1523.

Lo, E. Y., Shao, S. D. (2002). Simulation of near-shore solitary wave mechanics by an incompressible SPH method. Applied Ocean Research, 24(5), 275-286.

Lucy, L. B. (1977). A numerical approach to the testing of fusion process. Astronomical Journal, 88, 1013–1024.

Ma, Q. W. (2008). A new meshless interpolation scheme for MLPG_R method. CMES Computer Modeling in Engineering & Sciences, 23(2), 75-89.

Ma, Q. W., Zhou, J. T. (2009). MLPG_R method for numerical simulation of 2D breaking waves. CMES Computer Modeling in Engineering & Sciences, 43(3), 277-303.

Ma, Q. W., Zhou, Y., Yan, S. Q. (2016). A review on approaches to solving Poisson's equation in projection-based meshless methods for modelling strongly nonlinear water waves. Journal of Ocean Engineering and Marine Energy, 2(3), 279-299.

Monaghan, J. J., Lattanzio, J. C. (1985). A refined method for astrophysical problems. Astronomy & Astrophysics, 149(1), 135-143.

Monaghan, J. J. (2005). Smoothed particle hydrodynamics. Reports on Progress in Physics.

Quinlan N. J., Basa M., Lastiwka M. (2006). Truncation error in mesh-free particle methods. International Journal for Numerical Methods in Engineering, 66(13), 2064-2085.

Rafiee, A., Cummins, S., Rudman, M., Thiagarajan, K. (2012). Comparative study on the accuracy and stability of SPH schemes in simulating energetic free-surface flows. European Journal of Mechanics - B/Fluids, 36(10), 1-16.

Sibilla, S. (2015). An algorithm to improve consistency in smoothed particle hydrodynamics. Computers & Fluids, 118, 148-158.

Schwaiger, H. F. (2008). An implicit corrected SPH formulation for thermal diffusion with linear free surface boundary conditions. International Journal for Numerical Methods in Engineering, 75(6), 647-671.

Shao, S. D., Lo, E. Y. M. (2003). Incompressible SPH method for simulating newtonian and non-newtonian flows with a free surface. Advances in Water Resources, 26(7), 787-800.

Sriram, V,. Schlurmann, T., Schimmels, S. (2015). Focused Wave Evolution Using Linear and Second-Order Wavemaker Theory. Appl Ocean Res, 53, 279–296.

Sriram, V., Shagun, A., Schlurmann, T. (2020). Laboratory Study on Steep Wave Interaction with Fixed and Moving Cylinder. presented at the 30th Int Polar Ocean Eng Conf, virtual, ISOPE, I-20-3194.

Tamai T., Koshizuka S. (2014). Least squares moving particle semi-implicit method. Computational Particle Mechanics, 1(3), 277-305.

Tamai T., Murotani K., Koshizuka S. (2017). On the consistency and convergence of particle-based meshfree discretization schemes for the Laplace operator. Computers & Fluids, 142, 79-85.

Van der Vorst, H. A. (1992). Bi-CGSTAB: a fast and smoothly converging variant of Bi-CG for solution of non-symmetric linear system. Siam Journal on Scientific & Statistical Computing. 13, 631e644.

Violeau, D., Leroy, A. (2015). Optimal time step for incompressible SPH. Journal of Computational Physics, 288, 119-130.

Wang, L., Khayyer , A., Gotoh, H., Jiang, Q., Zhang, C. (2019). Enhancement of pressure calculation in projection-based particle methods by incorporation of background mesh scheme. Applied Ocean Research, 86, 320-339.

Yan, S. Q., Ma Q. W., Wang J. H. (2020). Quadric SFDI for Laplacian Discretisation in Lagrangian Meshless Methods. Journal of Marine Science and Application 19.3, 362-380.

Zhang, N. B., Zheng, X., Ma, Q. W., et al. (2018). A Hybrid Stabilization Technique for Simulating Water Wave--Structure Interaction by Incompressible Smoothed Particle Hydrodynamics (ISPH) Method. Journal of Hydro-environment Research., 18, 77--94.

Zhang, N. B., Zheng, X., Ma, Q. W. (2019) Study on wave-induced kinematic responses and flexures of ice floe by Smoothed Particle Hydrodynamics. Computers & Fluids. 189:46-59.

Zhang, G. M., Batra, R. C. .(2009). Symmetric smoothed particle hydrodynamics (ssph) method and its application to elastic problems. Computational Mechanics, 43(3), 321-340.

Zheng, X., Hu, Z., Ma, Q. W., Duan, W. Y. (2015). Incompressible SPH based on rankine source solution for water wave impact simulation. Procedia Engineering, 126, 650-654.

Zheng, X., Ma, Q. W., Duan, W. Y. (2014). Incompressible SPH method based on Rankine source solution for violent water wave simulation. Journal of Computational Physics, 276, 291-314.